International Journal of Chemical Studies

P-ISSN: 2349–8528
E-ISSN: 2321–4902
www.chemijournal.com
IJCS 2024; 12(1): 01-07

Received: 02-11-2023
Accepted: 10-12-2023

Dr. Ravi Kota
Assistant Professor, BITS-VIZAG, Andhra Pradesh, India

Dr. Sowbhagya Lakshmi Matcha
Assistant Professor, JNTU GV, Telangana, India

Dr. T Narasimhulu
Associate Professor, BITS-VIZAG, Andhra Pradesh, India

Corresponding Author:
Dr. Ravi Kota
Assistant Professor, BITS-VIZAG, Andhra Pradesh, India

Hydrothermal synthesis, characterization and biochemical applications of Fe_2O_3/RGO Nanocomposite

Dr. Ravi Kota, Dr. Sowbhagya Lakshmi Matcha and Dr. T Narasimhulu

Abstract
In this study, the author describes the synthesis of a binary nanocomposite, Fe_2O_3/RGO, through a straightforward and environmentally friendly hydrothermal process. To clarify the synthetic composite's structural and optical characteristics, it is thoroughly characterized using XRD, FTIR, FESEM-EDS, UV-DRS, and TGA. The produced composite is tested for photo catalysis, with an emphasis on the degradation of 4-nitrophenol (4-NP), a model dye pollutant, when exposed to visible light. Furthermore, the composite's antibacterial effectiveness is assessed against the *Bacillus subtilis* bacteria. The structural and morphological features of various examples are examined using FESEM, or scanning electron microscopy), revealing a nanofibrils structure reminiscent of pure Fe_2O_3. Photo catalytic activity is assessed by measuring 4-NP's deterioration, and the Fe_2O_3/RGO nanocomposite exhibits superior performance compared to experimental results with Fe_2O_3 alone. Under visible light irradiation, the nanocomposite uses H_2O_2 as a catalyst and in 50 minutes virtually completely (98%) degrades 4-NP. Interestingly, the research shows that the nanocomposite outperforms Fe_2O_3 in terms of antibacterial efficiency against gram-positive bacteria (*Bacillus subtilis*) at all three dilutions. These findings underscore the promising potential of the Fe_2O_3/RGO nanocomposite in both photo catalytic applications and antimicrobial interventions.

Keywords: Hydrothermal process, Nanocomposite, *Bacillus subtilis*, Photocatalytic applications

Introduction
The rapid pace of industrialization and urbanization has led to water contamination, primarily due to the discharge of different contaminants, including organic dyes, pesticides, and fungicides from industries. These pollutants present in effluents are known to be toxic, carcinogenic, and pose hazards to human health. Consequently, it becomes imperative to treat such wastewater before disposal. Presently, several wastewater treatment techniques are in use, but many of them are inefficient, costly, energy-intensive, leading to the production of substantial amounts of sludge [1, 2]. More than over the past two decades, AOP has become a viable technique for treating water. Advanced Oxidation Process (AOP) involves a method of photo catalysis that breaks down hazardous substances in water under light exposure, transforming them into carbon dioxide (CO_2), water (H_2O), and non-toxic compounds. As heterogeneous photo catalysts in AOP, metal oxides and their composites have drawn interest lately [3-5]. Fe_2O_3, known for its n-type semiconducting properties having a 2.2 eV indirect band gap, found diverse applications in areas such as pigments [6], gas sensors [7], and catalysis [8]. In the context of water treatment, Fe2O3 and its composites exhibit potential as effective photo catalysts in AOP, contributing to the degradation of pollutants and the remediation of contaminated water sources.
Nevertheless, to enhance the photo catalytic activity, the band gap of Fe_2O_3 has been mitigated through the creation of a composite with exceptional materials such as Graphene or polymers. Graphene, characterized by sp2 hybridization and a zero band gap, exhibits outstanding characteristics related to heat, structure, and catalysis, making it's a substance with promise, with numerous uses in energy storage, imaging, catalysis, and gas sensors [9, 10]. To the best of my knowledge, there aren't many reports on creating Fe2O3/RGO for use in photo catalysis. In this study, we report the synthesis of a Fe2O3/RGO magnetic reduced graphene oxide nanocomposite. The photo catalytic 4-nitrophenol breakdown process employs an a hydrothermal pathway in the presence of visible light. The Fe2O3/RGO nanocomposite hydrothermal synthesis for biological uses is examined in this work.

The author uses a variety of instrumental approaches to examine the morphology, structure, and thermal properties of the synthesized Fe2O3/RGO nanocomposite, including XRD, FTIR, TGA, UV-DRS, FESEM, and EDS. The diffraction planes (012), (104), (110), (113), (024), (116), (122), (214), (300), (208), (101), and (220) are assigned to According to Pure Fe2O3 (JCPDS, No. 33-0664), the diffraction peaks recorded at 2θ = 24.2°, 33.1°, 35.7°, 40.9°, 49.4°, 54.2°, 57.6°, 62.4°, 64.0°, 69.6°, 72.0°, and 75.5°, respectively.

Procedure for preparation

A. Selection of Materials

Sigma-Aldrich provided graphite powder with a particle size of +100 mesh. Without additional purification, the following compounds were utilized after being purchased from Merck in India: hydrogen peroxide (H2O2, 30 weight percent), sodium nitrate (NaNO3, 98 percent), concentrated sulfuric acid (H2SO4, 98 weight percent), potassium permanganate (KMnO4), hydrochloric acid (HCl, 37 percent), copper acetate (Cu(CH3COO)2), sodium hydroxide (NaOH), and zinc acetate dihydrate (Zn(CH3COO)2.2H_2O) and iron (II) chloride hexahydrate ($FeSO_4$.7H_2O) and iron (III) chloride hexahydrate (FeCl3.6H2O), zinc acetate dihydrate (Zn(CH3COO)2.2H2O). Organic compounds, including 2-nitrophenol, 4-nitrophenol, and methylene blue, were procured from Merck, India. To assess the antibacterial activity of the synthesized nanoparticles, *Bacillus subtilis* (MTCC211) and Escherichia coli (MTCC443) obtained from IMTECH, Chandigarh, India, were employed. The experiment was conducted using Milli-Q ultrapure water at all times.

B. Synthesis of Fe2O3/RGO nanocomposite

The 50 mg of graphene oxide (GO) were combined with a solution containing 10 mL of 0.1 M FeCl3·6H2O and 10 mL of an aqueous NaOH solution, then vigorously whisked for 30 minutes as part of a conventional synthesis technique. The final Slurry solutions were then placed inside Teflon-lined autoclaves and heated hydrothermally for an entire day at 180˚C. After being thoroughly washed with water, ethanol, and then water once more, the resultant yield was centrifuged.

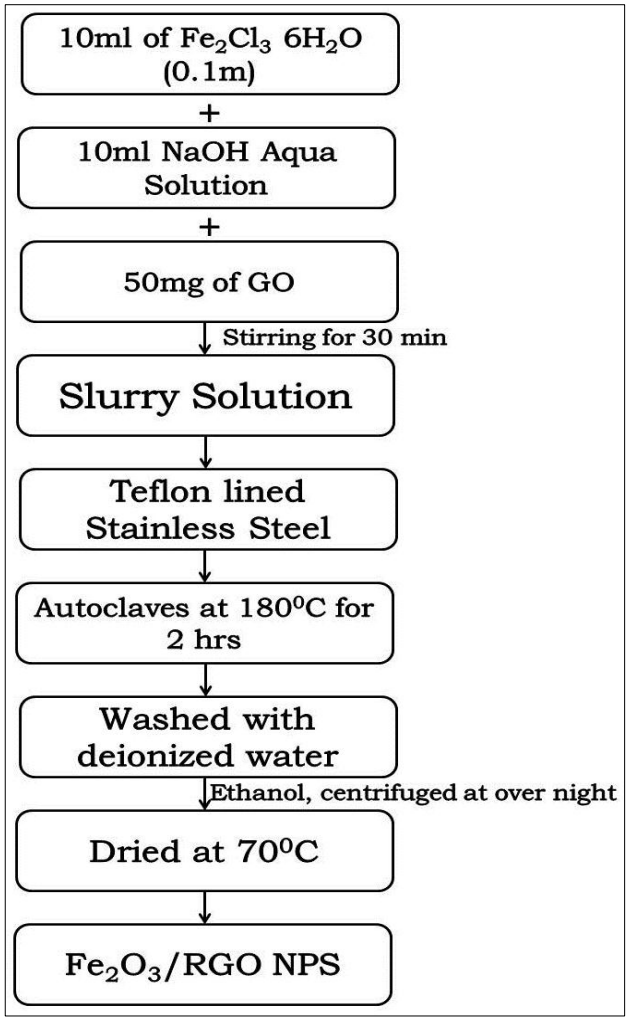

Fig 1: SynthesisofFe2O3/RGO nanoparticles.

Characterization

A. X-ray Diffraction

Figure 2(a) displays diffraction peaks at 2θ = 11° and 2θ = 43°, corresponding to the (002) and (100) reflections, respectively, that are representative of graphene oxide [11]. Diffraction peaks at 2θ = 24.2°, 33.1°, 35.7°, 40.9°, 49.4°, 54.2°, 57.6°, 62.4°, 64.0°, 69.6°, 72.0°, and 75.5° are displayed in Fig. 2(b), in accordance with Pure Fe_2O_3 (JCPDS, no. 33-0664) [12]. The diffraction planes with these peaks are correspondingly (012), (104), (110), (113), (024), (116), (122), (214), (300), (101), and (220).The principal diffraction peaks of the Fe_2O_3/RGO composite are comparable to those of pure Fe_2O_3, as demonstrated by XRD analysis, as seen in Fig. 2(c). This similarity suggests that the presence of Fe_2O_3 does not induce the formation of new crystal orientations or alter the preferred orientations of Fe_2O_3. New crystal orientations or alter the preferred Fe_2O_3.

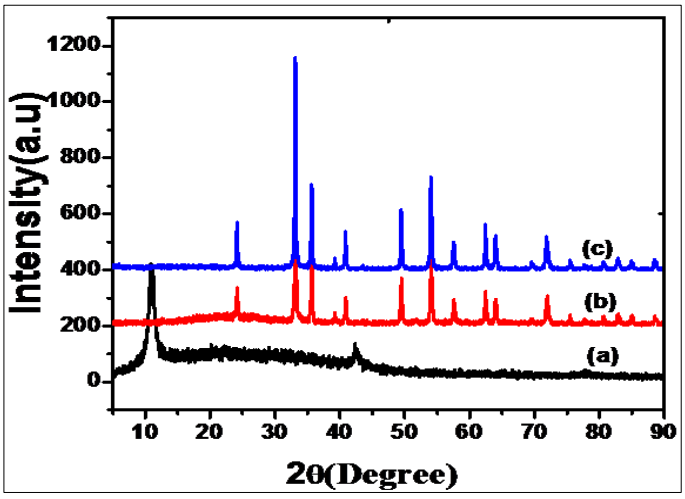

Fig 2: XRD patterns of (a) GO, (b) Fe2O3 and (c) Fe_2O_3/RGO

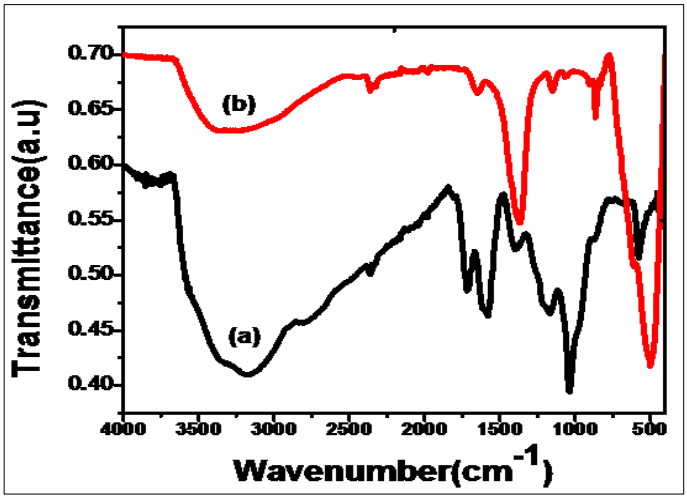

Fig 3: FTIR spectra of a) GO and b) Fe_2O_3/RGO

B. FTIR

With FTIR spectroscopy, the presence of oxygen-containing functionalities and changes during impregnation were investigated. The aromatic C=C group and the C=O group are represented by the peaks in the FTIR spectra of GO shown in Figure 3(a) at 1717.5 cm-1 and 1586 cm-1, respectively. The hydroxyl (-OH) group is indicated as a broad band with a centre at 3235.5 cm-1 [15]. Fig. 3(b) displays the Fe_2O_3/RGO composite's FTIR spectra after hydrothermal treatment. The metal oxide Fe-O is represented by a typical stretching vibration peak that is found at 514 cm−1. The O-H and C-O intensities decrease simultaneously, and the C=O peaks disappear. These changes suggest that GO has decreased and that functional groups containing oxygen have been removed.

C. FESEM-EDS

Scanning electron microscopy (FESEM) was used to examine the morphological characteristics and structure of different samples; the resulting pictures are shown in Fig. 4. A nanofibrils structure that resembles pure Fe_2O_3 is seen in Fig. 4(a). Fe_2O_3 is evenly dispersed and beautifully decorated on the surface of the reduced graphene oxide (RGO) sheets, as shown in Fig. 4(b). RGO sheets are exposed to Fe_2O_3, which causes them to exfoliate but stays intact, resulting in the formation of a composite material. Using energy-dispersive X-ray spectroscopy (EDS), the composition of the composite was ascertained from several areas. Peaks in the comparable EDS spectra shown in Fig. 4 (c) shows that Fe, O and C are present. The lack of further peaks indicates that the composite is free of contaminants. The combined is located.

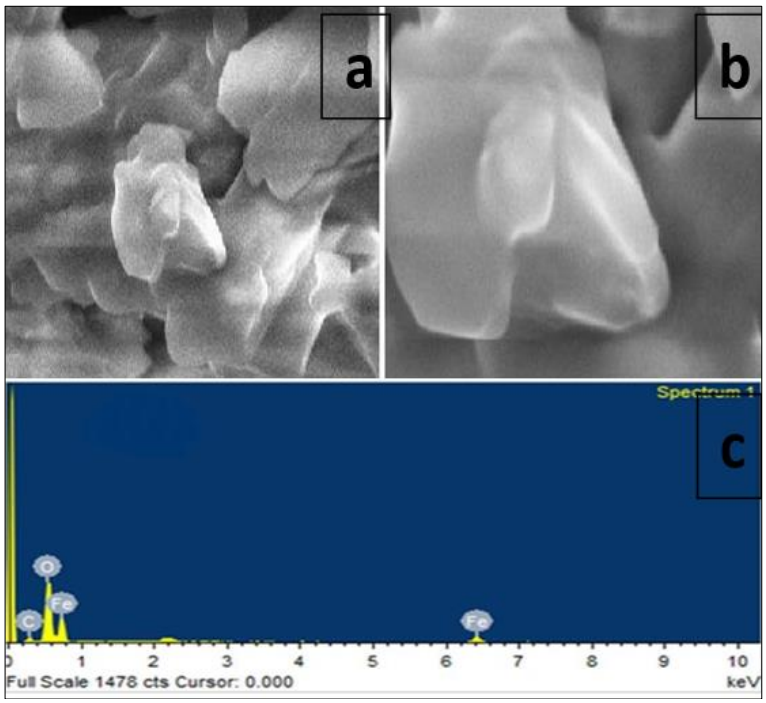

Fig 4: FESEM and EDS image of Fe_2O_3/RGO composite

D. Transmission Electron Microscope (TEM)

The TEM image of the Fe_2O_3/RGO composite is shown in Fig. 5. The results reveal that the Fe_2O_3/RGO composite exhibits a spherical shape and is agglomerated, with particle sizes ranging from 15 to 20 nm. Specifically, the Fe_2O_3/RGO composite reveals particles in a spherical form with a reduced particle size of 5 to 7 nm. When Fe_2O_3 is added to the surface of RGO sheets, the composite's particle size decreases and its

surface area increases, according to the collective results of these studies. The photo catalytic activity under visible light is subsequently enhanced as a result. Furthermore, the selected area electron diffraction (SAED) pattern in Fig. 5(c) indicates that the nanomaterial possesses a crystalline structure, aligning well with the XRD results. This observation reinforces the understanding of the composite's structural characteristics revealed through both TEM imaging and XRD analysis.

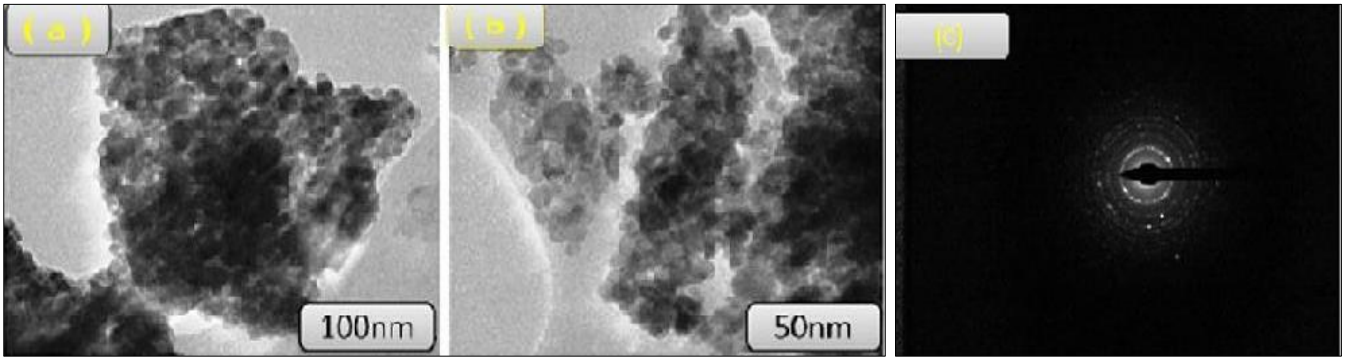

Fig 5: TEM image of a) Fe_2O_3, b) Fe_2O_3/RGO composite, (c) Selected area electron diffraction (SEAD)

Thermo gravimetric analysis

Fig. 6 displays the Fe_2O_3/RGO composite's TGA curves. The sample was heated at a rate of 10°C per minute while an air flow was present. Adsorbed water on the composite is thought to be evaporating, which accounts for the mass loss that has been seen between 25 and 200°C. The mass loss that occurs between 200 and 350°C is thus ascribed to the elimination of functional groups that contain oxygen. Notably, the temperature range of 350 to 800°C has a significant mass loss, indicative of the pyrolysis of the carbon skeleton [18]. The significant mass loss that occurs between 350°C and 800°C indicates that the calcinations procedure was successful in reducing graphene oxide (GO) to reduced graphene oxide (RGO). This finding emphasizes how effective the reduction ion process in transforming GO into its reduced form.

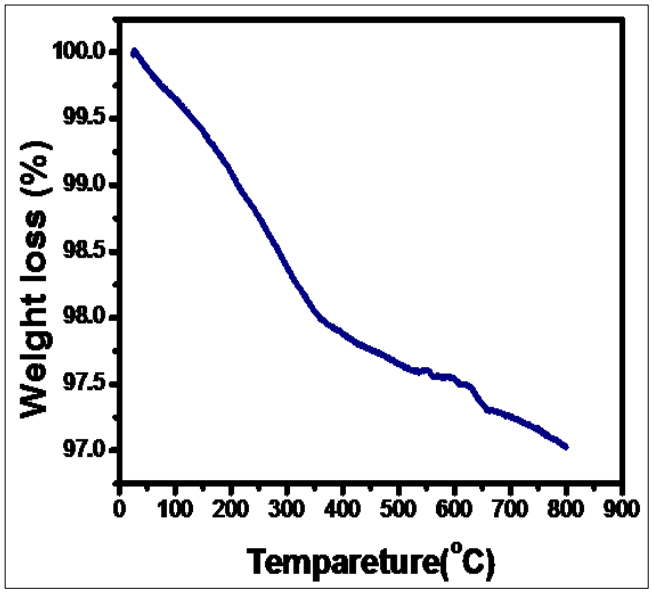

Fig 6: TGA curve of Fe_2O_3/RGONC

UV-DRS

The normalized UV- vis /DRS spectra of the Fe_2O_3 / RGO composite and pure Fe_2O_3 are shown in figs. 7(a) and (b). The catalyst's band gap energy (Eg) can be calculated with the help of the following formula:

$$Eg\ (eV) = 1240 / \lambda$$

Where, 'Eg' is the band gap energy, 'λ' is the wavelength (nm) corresponding to the absorption.

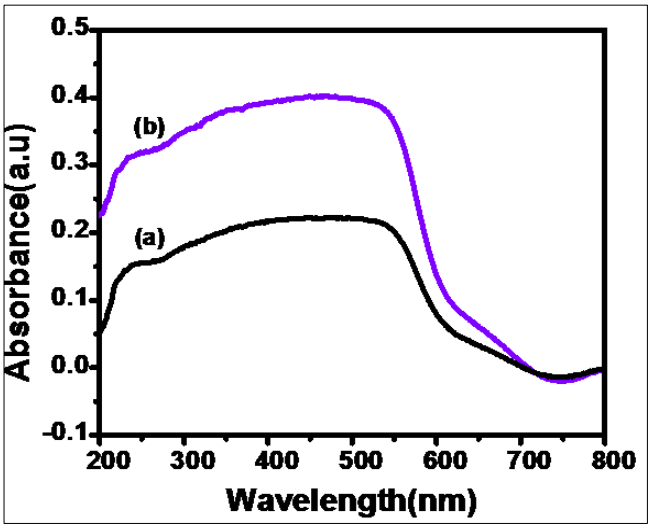

Fig 7: UV-DRS of (a) Fe_2O_3 and (b) Fe_2O_3 / RGONC

In the UV-visible absorption spectra, 1.98 eV (625 nm) is the band gap energy of pure Fe_2O_3. On the other hand, 1.85 eV, or 670 nm, is the lower band gap energy of the Fe_2O_3/RGO composite [19]. When compared to pure Fe_2O_3, the Fe_2O_3/RGO composite exhibits greater absorption intensity at 670 nm and a shift in absorption edge to the more visible range at 625 nm. The interaction between Fe, O, and C in the Fe_2O_3/RGO composite is responsible for this change. As a result, it is confirmed that pure Fe_2O_3 and RGO together work effectively to enhance photo catalytic activity in response to visible light.

Results and Discussions

A. Photo catalytic activity of prepared nanocomposite:

The photo catalytic degradation of 4-nitrophenol (4-NP) under visible light irradiation was investigated using both the Fe_2O_3/RGO nanocomposite and pure Fe_2O_3. After 120 minutes of photo catalytic activity, pure Fe_2O_3 first only showed a 29% degradation of 4-NP, as seen in Fig. 8(a).Then, under various circumstances, the Fe_2O_3/RGO nanocomposite was used to degrade 4-NP. When subjected to a solution with an acidic pH (pH-4) for 120 minutes and a basic pH (pH-10) for 70 minutes, the nanocomposite exhibited improved photo

catalytic activity, reaching 57% and 77% degradation, respectively (Fig. 8 (b, c)).

Notably, the nanocomposite demonstrated superior performance in a basic solution (pH-10) compared to an acidic environment (pH-4). In the final phase, H_2O_2 was introduced to the Fe_2O_3/RGO nanocomposite during the photo catalytic process. The nanocomposite, under these conditions, achieved almost complete degradation (98%) of 4-NP within 50 minutes, as depicted in Fig. 8 (d). This result underscores the enhanced photo catalytic efficiency of the nanocomposite, particularly in the presence of H_2O_2, making it a promising candidate for effective pollutant degradation. Using both the Fe_2O_3/RGO nanocomposite and pure Fe_2O_3, the photo catalytic degradation of 4-nitrophenol (4-NP) under visible light irradiation was studied. As shown in Fig. 8(a), pure Fe_2O_3 initially only demonstrated a 29% degradation of 4-NP after 120 minutes of photo catalytic activity. Then, the Fe_2O_3/RGO nanocomposite was employed to break down 4-NP under diverse conditions. Following their interaction with dye molecules on the composite surface, these radicals degrade the dye molecules into products like CO_2 and H_2O (Equations 1-4). [20].

$$Fe_2O_3 / RGO + light \; h^+ + e^- \quad \text{Eq. (1)}$$

$$H_2O + h^+ \longrightarrow {}^{\cdot}OH \quad \text{Eq. (2)}$$

$$H_2O + e^- \longrightarrow {}^{\cdot}O_2^- \quad \text{Eq. (3)}$$

$$Fe_2O_3/RGO + light \longrightarrow h^+ + e^- \quad \text{Eq. (4)}$$

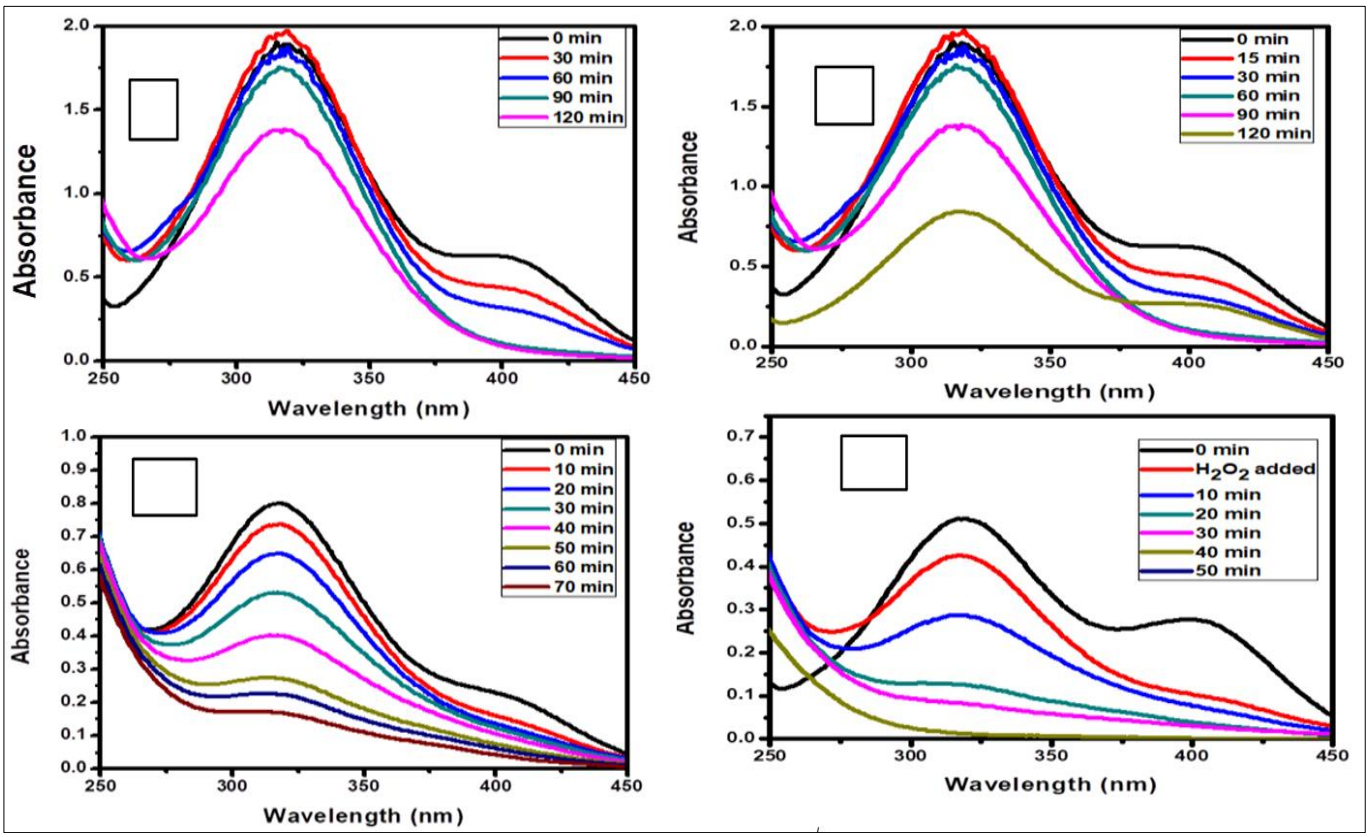

Fig 8: Photo catalytic degradation of 4-NP by a) Fe_2O_3, b) Fe_2O_3/RGO NC (pH-4), c) Fe_2O_3/RGO NC (pH-10) and d) Fe_2O_3/RGONC+H_2O_2

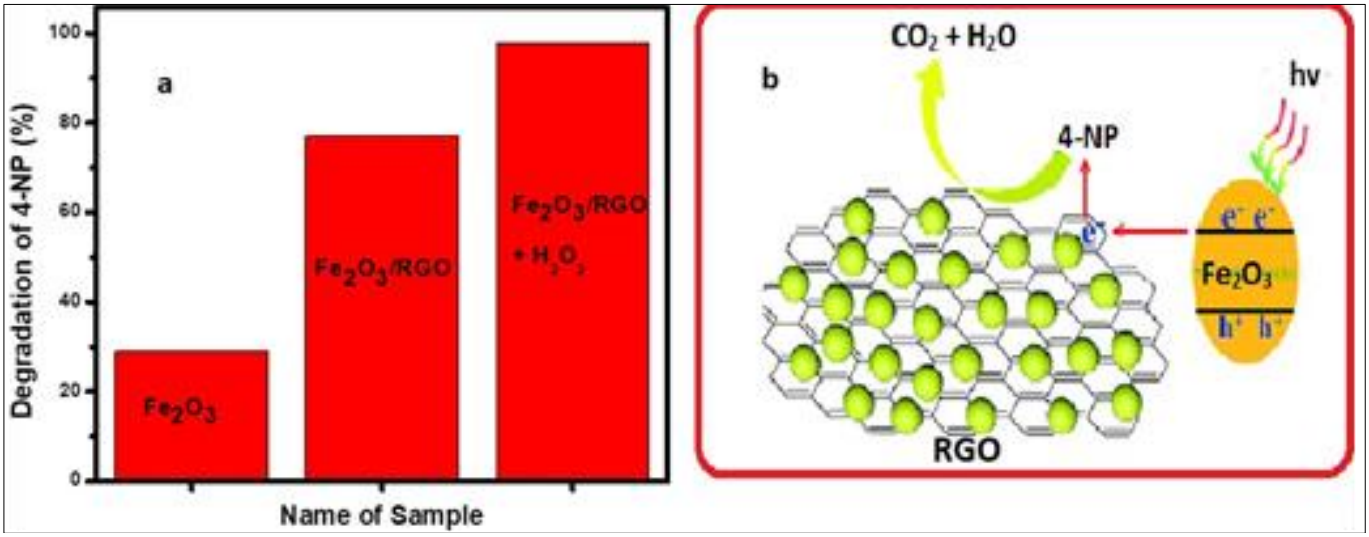

Fig 9(a): Degradation efficiency of prepared samples, (b) Photo catalytic degradation mechanism

Table 1: Shows the zone of inhibition over *B. subtilis*

Organism	Test Compound	25 mg/ ml	10 mg/ ml	5 mg/ ml	Standard 10 mg/ml
B. subtilis	Fe_2O_3	--	--	--	32
	Fe_2O_3/RGO	18	15	16	32

b. Anti-microbial activity of prepared nanocomposite

The antimicrobial activity of the prepared samples, including Fe_2O_3 and the Fe_2O_3/RGO composite, is illustrated in Fig. 10. Table 1 provides details on the zone of inhibition against *B. subtilis*. The findings unequivocally indicate that the Fe_2O_3/RGO composite exhibits notable antimicrobial efficacy against the Gram-positive bacteria (*B. subtilis*) exceeding Fe_2O_3's antibacterial efficacy in all three dilutions. Applications for metal oxide nanoparticles are numerous and include environmental cleanup, optoelectronic materials, sensors, and catalysis [21]. For many applications, regulated synthesis of these nanoparticles is essential, and solution phase approaches become indispensable instruments because they provide a high level of control over the synthesis products [22].

c. Mechanism of action of composite on Bacteria

The photo catalytic degradation of 4-nitrophenol (4-NP) under visible light irradiation was investigated using both the Fe_2O_3/RGO nanocomposite and pure Fe_2O_3. After 120 minutes of photo catalytic activity, pure Fe_2O_3 first only showed a 29% degradation of 4-NP, as seen in Fig. 8(a).Subsequently, the Fe_2O_3/RGO nanocomposite was utilized to degrade 4-NP in various circumstances. Moreover, the water's oxygen and negative charges combine to form superoxide radicals, which disturb coenzyme-independent respiration, cell wall construction, and ion homeostasis [26]. The Fe_2O_3/RGO nanocomposite enhances the peroxidation of the polyunsaturated phospholipid component of the lipid membrane, thereby promoting disruption in cell respiration and leading to cell death [27].

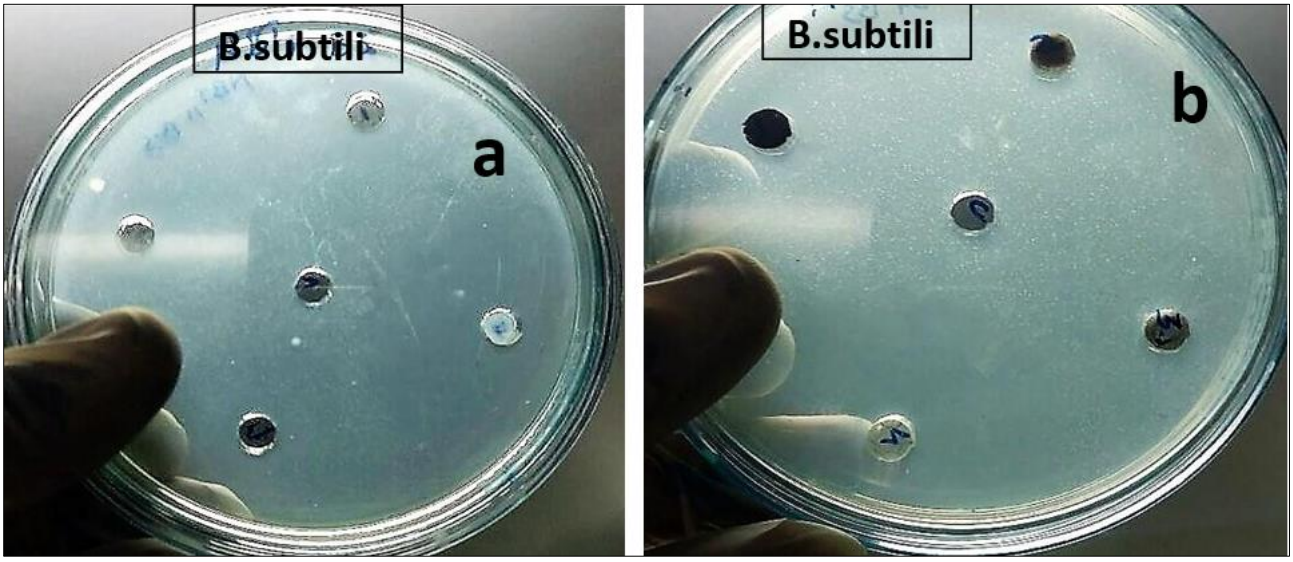

Fig 10: Anti-microbial activity of (a) Fe_2O_3 and (b) Fe_2O_3 /RGONC

Conclusion

This paper details the hydrothermal synthesis of a Fe_2O_3/RGO nanocomposite (NC) and examines it's structural, morphological, and thermal properties using a range of analytical techniques, including XRD, FTIR, TGA, UV-DRS, FESEM, and EDS. The photo catalytic activity of the synthesized Fe_2O_3/RGO NC is evaluated by means of 4-nitrophenol (4-NP) degradation. A comparison with Fe_2O_3 experimental results indicates that the Fe_2O_3/RGO NC exhibits remarkable photo catalytic activity, particularly when using H_2O_2, for the degradation of 4-NP under visible light irradiation. Fascinatingly, in all three dilutions, the nanocomposite shows strong antibacterial activity against gram-positive bacteria (*Bacillus subtilis*) in contrast to Fe_2O_3.

References

1. Tuzen M. Toxic and essential trace elemental contents in fish species from the Black Sea, Turkey. Food and chemical toxicology. 2009 Aug 1;47(8):1785-90.
2. Hegab HM, Zou L, Membr J. Sci. 2015;484:95-106.
3. Zou M, Feng L, Ganeshraja AS, Xiong F, Yang M. Defect induced nickel, nitrogen-codoped mesoporous TiO2 microspheres with enhanced visible light photocatalytic activity. Solid State Sciences. 2016 Oct 1;60:1-0.
4. Sundaram GA, Kanniah R, Li K, Zhu X, Subramani T, Xu W, *et al*. RSC Advances. 2016;6:72791–802.
5. Wang DH, Jia L, Wu XL, Lu LQ, Xu AW. One-step hydrothermal synthesis of N-doped TiO 2/C nanocomposites with high visible light photocatalytic activity. Nanoscale. 2012;4(2):576-84.
6. Dirk W. Characterization of synthetic hydrous hematite pigments. Thermochimica acta. 2006 Jun 15;445(2):195-9.
7. Chen J, Xu LN, Li W, Gou X. α-Fe2O3 nanotubes in gas sensor and lithium-ion battery applications. Advanced Materials. 2005 Mar 8;17(5):582-6.
8. Osama S, Wolfgang R, Achim S, Grigorios K, Robert Angew. Styrene synthesis: high conversion over unpromoted iron oxide catalysts under practical working conditions. Angewandte Chemie International Edition. 2003 Dec 1;42(46):5760-3.
9. Geim AK, Novoselov KS. The rise of graphene. Nature materials. 2007 Mar;6(3):183-91.
10. Service RF. Carbon sheets an atom thick give rise to graphene dreams, Science. 2009;324(5929)875–877.

11. Zhao Y, Song X, Song Q, Yin Z. A facile route to the synthesis copper oxide/reduced graphene oxide nanocomposites and electrochemical detection of catechol organic pollutant. CrystEngComm. 2012;14(20):6710-9.
12. Wang SB, Wang W, Zhan P, Jiao SQ, Chem Electro Chem. 2014;1:1636–1639.
13. Liu XJ, Pan LK, TL V, Zhu G, Lu T, Sun Z, Sun CQ, RSC Adv. 2011;1:1245–1249.
14. Xinjuan Liu, Taiqiang Chen, Haipeng Chu, Lengyuan Niu, Zhuo Sun, Likun Pan, Chang Q. Sun, Electrochimica Acta. 2015;166:12-16.
15. Chandra V, Park J, Chun Y, Lee JW, Hwang IC, Kim KS, ACS Nano. 2010;4:3979-3986.
16. Fu YS, Wang X. Ind, Eng. Chem. Res., 2011;50:7210-7218.
17. Jeong HK, Lee YP, Jin MH, Kim ES, Bae JJ, Lee YH. Chem. Phys. Lett. 2009;470:255-258.
18. Cornell RM, Schwertmann U. TheIron Oxide Book, 2nded. Wiley-VCH: Weinheim, Germany. 2003, 147.
19. Soltani N, Saion E, Yunus WM, Erfani M, Navasery M, Bahmanrokh G, *et al*. Enhancement of visible light photocatalytic activity of ZnS and CdS nanoparticles based on organic and inorganic coating. Applied Surface Science. 2014 Jan 30;290:440-7.
20. Carmela Aprile, Elena Gobechiya, Johan Martens A, Paolo Pescarmona P. New mesoporous composites of gallia nanoparticles: high-throughput synthesis and catalytic application. Chemical communications. 2010;46(41):7712-4.
21. Jennifer Dahl A, Bettye LS, Maddux E. James Hutchison, Chem. Rev. 2007;107(6):2228–2269.
22. Sunada K, Watanabe T, Hashimoto K. Journal of Photochemistry and Photobiology A: Chemistry. 2003;156(1-3):227–233.
23. Carp O, Huisman CL, Reller A. Progress in Solid State Chemistry. 2004;32(1-2):33-177.
24. Trunina NA, Darvin ME, Kordás K, Sarkar A, Mikkola JP, Lademann J, *et al*. Monitoring of TiO $ _ {\bf 2} $ and ZnO Nanoparticle Penetration Into Enamel and Dentine of Human Tooth *in vitro* and Assessment of Their Photocatalytic Ability. IEEE Journal of Selected Topics in Quantum Electronics. 2013 Aug 2;20(3):133-40.
25. Kubacka A, Diez MS, Rojo D, Bargiela R, Ciordia S, Zapico I, *et al*. Understanding the antimicrobial mechanism of TiO2-based nanocomposite films in a pathogenic bacterium. Scientific reports. 2014 Feb 19;4(1):4134.